Journal of Alloys and Compounds 513 (2012) 224–229

Contents lists available at SciVerse ScienceDirect

Journal of Alloys and Compounds

journal homepage: www.elsevier.com/locate/jallcom

Synthesis and characterization of Sn-rich Ni–Sb–Sn nanosolders

Ratikanta Mishra [a], Adela Zemanova [b], Ales Kroupa [b], Hans Flandorfer [a], Herbert Ipser [a,*]

[a] University of Vienna, Department of Inorganic Chemistry/Materials Chemistry, Waehringerstr. 42, A-1090 Wien, Austria
[b] Institute of Physics of Materials, Academy of Sciences of the Czech Republic, CZ-61662 Brno, Czech Republic

ARTICLE INFO

Article history:
Received 18 August 2011
Received in revised form 9 October 2011
Accepted 10 October 2011
Available online 18 October 2011

Keywords:
Metals and alloys
Nanostructured materials
Nanosolders
Lead-free soldering
Chemical synthesis
Surface enthalpy

ABSTRACT

Nano-crystalline samples of pure Sn and of Sn-rich ternary Ni–Sb–Sn alloys, with compositions ranging from 80 to 97.5 at% Sn and a Ni to Sb molar ratio of 1:1, were synthesized by reduction of stoichiometric metal chloride solutions with $NaBH_4$ at 0 °C in alkaline medium. The particle sizes of the obtained alloys, measured by TEM/SEM, were found to be in the range of 40–350 nm. A relative decrease in melting temperature of up to 15 °C was observed for these alloys compared to a bulk sample. A sample with 95 at% Sn was subjected to heat treatment at 180 °C for various time periods up to 5.0 h to study particles with well defined average sizes between 50 and 135 nm. The melting temperatures of the annealed samples were found to increase progressively with increasing particle size. At the same time, the excess surface energy of these heat treated samples was measured as a function of particle size using a Calvet-type calorimeter. From the differences of the $(H_{573}–H_{299})$ values between nano and bulk samples, the excess enthalpies for nano-sized samples were derived to be between 18.8 ± 1.9 and 0.8 ± 1.4 kJ g^{-1} for particle sizes between 50 and 135 nm.

1. Introduction

The physical, electronic and thermodynamic properties of alloys in their nanoform are significantly different from those of the corresponding bulk materials. It is the surface energy in these nanomaterials that assumes significance, due to the presence of a higher number of atoms at the surface compared to the bulk material. The difference in properties of materials with particles in the nanometer size regime (1–100 nm) compared to bulk materials can be related to the excess surface energy [1–3]. For example, a depression of the melting temperature of nanoparticles has been reported by many authors [4–8]. Various quantitative relationships between the melting temperature and the particle size have been developed, among others, by Pawlow [9], Buffat and Borel [10], Borel [11], Dick et al. [12], Nanda et al. [13], Jiang et al. [14], and Qi and Wang [15]. Likewise, a decrease of the Curie temperature, the reduction of magnetic moments, and an improved magneto-caloric effect for magnetic refrigeration has been reported for magnetic nanoparticles [16–18]. In semiconductors, the band gap increases with the decrease of particle size, and it is highly significant when the particle sizes are comparable to or below the exciton Bohr radius [19,20]. Nanocrystals exhibit an intermediate behavior between bulk and isolated molecules. The knowledge of excess thermodynamic parameters such as excess enthalpy and entropy is important in predicting the above properties of nanomaterials.

Sb–Sn based alloys are possible candidates for new high-temperature solders. The melting temperatures, mechanical properties and quality of joints formed by these materials with different substrates can be modified by alloying with additional elements. There are continuing attempts to reduce the particle size in solder powders in order to reduce the melting temperature of solder alloys, especially in reflow soldering. Currently, the smallest commercial particle size for lead-free solders seems to be in the range between 2 and 8 μm (Type 8) [21] which is still far from the nanometer size where a size dependent reduction of the melting temperature would come into play. In this work we report synthesis and characterization of Sn-rich Ni–Sb–Sn nanoalloys with melting temperatures that are noticeably reduced compared to the bulk alloy. We also report the determination of the excess surface energy of the Ni–Sb–Sn nanoalloys as a function of particle size.

2. Experimental

Nanopowders of Sn and Sn-rich Ni–Sb–Sn alloys were synthesized following the procedure described by Yang et al. [22]. In the first step aqueous stock solutions of $SnCl_2$ (0.08 M), $SbCl_3$ (0.03 M), and $NiCl_2$ (0.06 M) were prepared by dissolving $SnCl_2{\cdot}2H_2O$ and $SbCl_3$ (Alfa Aesar, 99.99% purity) in diluted hydrochloric acid (5 M), and $NiCl_2{\cdot}6H_2O$ (Alfa Aesar, 99.9985% purity) in distilled water. Appropriate volumes of the above metal chloride solutions were mixed together to make compositions with Sn contents varying from 80 to 97.5 at% and with a Ni to Sb molar ratio of 1:1. To the resulting solutions required amounts of a 1 M solution of tri-sodium citrate was added as chelating reagent. A 0.5 M $NaBH_4$ stock solution was prepared at a pH value of 14 from a 4.4 M $NaBH_4$ stable solution obtained from Alfa Aesar. The two separate aqueous solutions were cooled to 0 °C in ice water before reaction.

* Corresponding author. Tel.: +43 1 4277 52906; fax: +43 1 4277 9529.
E-mail address: herbert.ipser@univie.ac.at (H. Ipser).

0925-8388/$ – see front matter © 2011 Elsevier B.V. All rights reserved.
doi:10.1016/j.jallcom.2011.10.023

40 ml of metal chloride solution was added drop wise within 10 min to 40 ml of the $NaBH_4$ solution under strong magnetic stirring. With continued addition, the color of the solution turned brown with formation of some bubbles which was followed by the appearance of some black suspensions. The mixed solutions were stirred for another 30 min, and for the entire period the reaction vessel was cooled in ice water. The resultant suspensions were separated by centrifuge and rinsed several times with distilled water and acetone. The precipitate was dried under vacuum at room temperature.

The fine black powder samples obtained in this way were characterized by X-ray diffraction (XRD), differential scanning calorimetry (DSC), and electron microscopic techniques. To make particles with different crystallite sizes, an alloy with composition $Ni_{2.5}Sb_{2.5}Sn_{95}$ was synthesized following the procedure described above. Individual parts of it (about 200 mg) were sealed in evacuated quartz ampoules and annealed at 180 °C for 0.5, 1.0, 1.5, 2.0, 3.0, and 5.0 h. During sealing, extreme care was taken in order not to increase the temperature of the samples but to keep them at room temperature. After the annealing experiments, the change in morphology, crystal size, particle size, and the melting temperatures of the samples were determined using optical microscopy, XRD, scanning electron microscopy (SEM), transmission electron microscopy (TEM), and DSC techniques. The powder patterns of the samples were recorded on a Bruker D8 diffractometer in $\theta/2\theta$ geometry (reflection setting) equipped with a one-dimensional silicon strip detector using Cu $K_{\alpha 1}$ radiation. The unit cell parameters were refined using the program TOPAS V3 [23]. High purity silicon was used as internal standard for the lattice parameter determination.

Scanning electron microscopy (SEM) equipped with FIB (focused ion beam) was used to observe the morphologies of the synthesized nanoparticles (Tescan Lyra 3 FEG_FIB, Tescan, Brno, Czech Republic), applying an accelerating potential of 15 kV. SEM specimens were prepared by a two-stage replica method. The Ni–Sb–Sn nanoalloys were dispersed in collodion on a slide. After drying, a carbon film supported by a copper grid (150 meshes) was applied onto the sample. Then the sample with the copper grid was carburized and the collodion was dissolved in an amyl acetate solution.

DSC measurements were carried out on a DSC 404S/3 (Netzsch, Selb, Germany) in alumina crucibles under the flow of Ar gas. The apparatus was evacuated and flushed with purified Ar several times before heating. About 50 mg of the powder samples was pressed into a pellet with 5 mm diameter at a pressure of 10 bars. Two heating- and cooling curves were recorded for each sample using a heating rate of 10 K min^{-1}. The temperature calibration of the DSC instrument was done at the melting points of high purity In, Sn, Ag and Au under identical experimental conditions.

Measurements of the heat content ($H_{573}-H_{299}$) of the samples were carried out in a Calvet-type micro-calorimeter (SETARAM, Lyon, France). The heat flow signal in the calorimeter is measured by the help of a thermopile with more than 200 thermocouples. The wire wound resistance furnace is suitable for measurements up to 1000 °C, and the calorimeter is equipped with an automatic sample drop device for 30 drops. Data acquisition, control, and data evaluation were performed using the computer programs LabView and HiQ as described by Flandorfer et al. [24]. The samples, in the form of pellets, were maintained at 299 ± 0.5 K in the sample holder and were then dropped into the sample cell equilibrated at the experimental temperature of 573 K. During the experiments a flowing Ar atmosphere (approximately 60 cm^3 min^{-1}) was maintained to prevent oxidation. At the end of each series the calorimeter was calibrated by five additions (approximately 40 mg each) of standard Al_2O_3 (NIST SRM-720) supplied by the National Institute of Standards and Technology (NIST), Gaithersburg, MD, USA. The temperature of the isothermal block (DT) and the sample temperature in the furnace T were measured using a Pt–Pt 10% Rh thermocouple and thermoresistors for each drop. The accuracy is usually better than ±1 °C. The heat flow signal for each experiment was recorded for 30 min before dropping a new sample.

3. Results and discussion

3.1. Characterization by XRD and DSC

The XRD analyses of the Ni–Sb–Sn nanoalloy samples show that the major phase for all compositions is tetragonal (Sn) with space group $I4_1/amd$ (see Table 1). However, for samples with Sn contents of less than 95 at%, two additional co-existing phases were found, i.e. monoclinic Ni_3Sn_4 (space group $C2/m$), and the trigonal β phase (~SbSn, space group R-3m) which is in agreement with our recent experimental phase diagram investigation of the Sn-rich corner [25]. The appearance of the β phase in a sample with an Sb content of 3.75 at% might indicate that the solubility of Sb in (Sn) has decreased from about 6 at% at 200 °C [25] to less than 3.75 at% at 0 °C although this sample, prepared at 0 °C, is not necessarily in an equilibrium state. The XRD lines for Ni_3Sn_4 and the β phase are found to be broader and more diffuse compared to the lines due to (Sn). The intensities of the XRD peaks due to Ni_3Sn_4 and the β phase were found to increase with a decrease in Sn content indicating the formation of higher amounts of these phases at lower Sn contents. Fig. 1 shows the XRD patterns of samples with 80, 90, 95, and 100 at% Sn and a molar ratio 1:1 of Ni to Sb, demonstrating the evolution of Ni_3Sn_4 and β-phase with decreasing Sn content. Table 1 gives cell parameters and the relative average crystallite size of the different co-existing phases derived from the refinement of the XRD data under similar refinement conditions. It can be observed that the crystallite size of the major phase (Sn) decreases with a decrease in the Sn content of the sample.

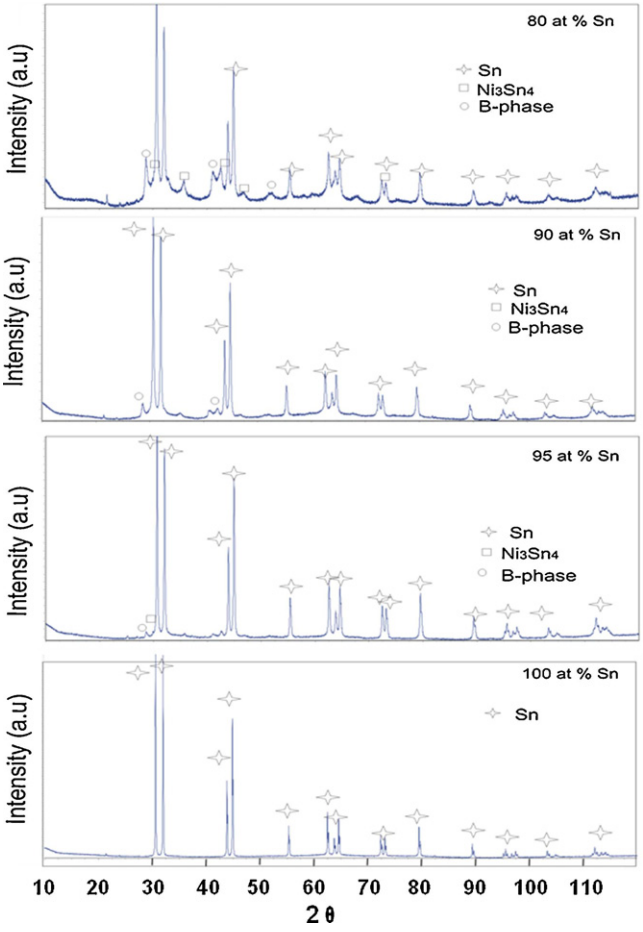

Fig. 1. XRD patterns of four nano-sized samples containing 80, 90, 95, and 100 at% Sn; samples with less than 100 at% Sn contain besides Sn also traces of Ni_3Sn_4 and of the β-phase (SbSn).

As an example, SEM images of Ni–Sb–Sn nanoalloys with four different Sn contents are shown in Fig. 2a–d. The particles have approximately spherical shape, and their average sizes are found to be 45, 60, 85, and 195 nm, respectively, for Sn contents of 80, 87.5, 92.5, and 100 at% Sn. Considering all error limits, the agreement with the sizes determined from XRD in Table 1 is good, except for the one sample with pure Sn.

Fig. 3 shows the DSC melting peaks for the sample with 95 at% Sn recorded at a heating rate of 10 K min^{-1}. This relatively fast heating rate was chosen in order to avoid sintering of the alloy as far as possible. In the first heating segment, a clear endothermic peak appeared with an onset at 221 °C which was related to the first appearance of a liquid phase. On repeating the thermal cycle, an increase of 11 °C was observed for the onset temperature of this peak. (Note that the onset temperature was taken for the appearance of the first liquid for better comparison although the melting behavior of alloys in the Sn-rich corner is rather complicated [25].)

Table 1
Results of XRD and DSC measurements of Ni–Sn–Sb nanoalloys.

Composition	Phases	Amount[a] (%)	Cell parameters (Å)	Crystallite size (XRD) (nm)	Melting temp. (onset[b]) 1st heating (°C)	Melting temp. (onset[b]) 2nd heating (°C)	Difference between 1st and 2nd heating (°C)
Sn_{100}	Sn	100	a = 5.82988(4) c = 3.18001(2)	345	227.5	231.5	4
$Sn_{97.5}Ni_{1.25}Sb_{1.25}$	(Sn)	100	a = 5.83117(4) c = 3.18093(3)	150	225	232	7
$Sn_{95}Ni_{2.5}Sb_{2.5}$	(Sn)	~97	a = 5.83161(7) c = 3.18121(4)	75	221.0	232	11
	Ni_3Sn_4	~3	–	–			
$Sn_{92.5}Ni_{3.75}Sb_{3.75}$	(Sn)	95	a = 5.8329(4) c = 3.1820(2)	65	217.5	232	14.5
	Ni_3Sn_4	5	a = 12.98(1) b = 3.844(2) c = 5.326(2) β = 107.9°	20			
$Sn_{90}Ni_5Sb_5$	(Sn)	80	a = 5.8316(1) c = 3.1805(9)	65	217.5	232	14.5
	Ni_3Sn_4	20	a = 13.37(3) b = 3.818(3) c = 5.246(3) β = 108.8°	15			
$Sn_{87.5}Ni_{6.25}Sb_{6.25}$	(Sn)	65	a = 5.8328(1) c = 3.1811(1)	60	217	232	15
	Ni_3Sn_4	20	a = 12.174(9) b = 4.062(5) c = 5.080(6) β = 104.7°	<10			
	β-Phase	15	a = 4.392(3) c = 5.399(7)	30			
$Sn_{82.5}Ni_{8.75}Sb_{8.85}$	(Sn)	50	a = 5.833(1) c = 3.1823(6)	85	217.5	232	14.5
	Ni_3Sn_4	30	a = 11.86(1) b = 4.145(4) c = 5.920(4) β = 99.7°	<10			
	β-Phase	20	a = 4.389(6) c = 5.41(1)	40			
$Sn_{80}Ni_{10}Sb_{10}$	(Sn)	45	a = 5.8322(2) c = 3.1807(1)	45	216.5	232	15.5
	Ni_3Sn_4	30	a = 12.217(9) b = 4.033(2) c = 5.118(3) β = 104.7°	<10			
	β-Phase	25	a = 4.39(3) c = 5.38(9)	40			

[a] The amount was derived from the refinement of the XRD data of the samples; the corresponding error is estimated to be about 10%.
[b] Although the melting behavior of Sn-rich ternary Ni–Sb–Sn samples is rather complicated [25] the onset of the first effect on heating was taken in order to allow for a better comparison.

However, no difference in onset temperature could be observed for the corresponding peak in the cooling cycle.

The difference in the onset temperature of this peak in the first and second heating segment can be explained by the fact that, in first heating, most of the particles are still in a nanocrystalline form which has a lower melting temperature compared to the bulk sample. During cooling and reheating, the samples have re-crystallized as bulk material, and the thermal effect is due to the melting of bulk samples with normal crystallite sizes. On the other hand, in the cooling stage samples freeze in both cycles from the same liquid state, so they exhibit the same (somewhat super cooled) onset temperature. This phenomenon of a decrease of the melting temperature of nanoparticles compared to their corresponding bulk materials, regardless of the nature of the materials, has been reported in the past by several authors [4–8]. Table 1 gives the absolute temperatures as well as the difference in the onset temperature of the melting peak between first and the second cycle for samples with Sn contents between 80 and 100 at%. It was further observed that, as the compositions of the samples move farther away from pure Sn, the intensity of the melting peak decreases progressively.

XRD analyses of individual parts of the alloy $Sn_{95}Ni_{2.5}Sb_{2.5}$, annealed at 180 °C for periods of 0.5, 1.0, 1.5, 2.0, 3.0, and 5.0 h, showed that the samples were almost single phase with small amounts of the Ni_3Sn_4 phase. The crystallite size obtained from the refinement of the XRD data of the annealed samples also indicated that the average crystal size was progressively increasing with the annealing period. Fig. 4 shows the SEM pictures for this particular alloy after different periods of annealing. The average particle sizes for these samples were found to be 55, 70, 95, 105, 120 and 135 nm, respectively, which agrees quite well with the sizes obtained from the XRD measurements.

Fig. 5 gives the DSC plots for the corresponding samples. The onset temperatures of the melting peak for the annealed samples were found to increase progressively with an increase in particle size, i.e. 221, 222.5, 223.5, 225.5, 227.5, 228.5 and 230.0 °C for samples annealed at 180 °C for periods of 0, 0.5, 1.0, 1.5, 2.0, 3.0, and 5.0 h, respectively. The average onset temperature for all the heat treated samples in the second heating cycle was found to be 232 ± 0.5 °C. Thus, the depression in the onset temperature of the melting peak (ΔT) for $Sn_{95}Ni_{2.5}Sb_{2.5}$ was 11, 9.5, 8.5, 6.5, 4.5, 3.5,

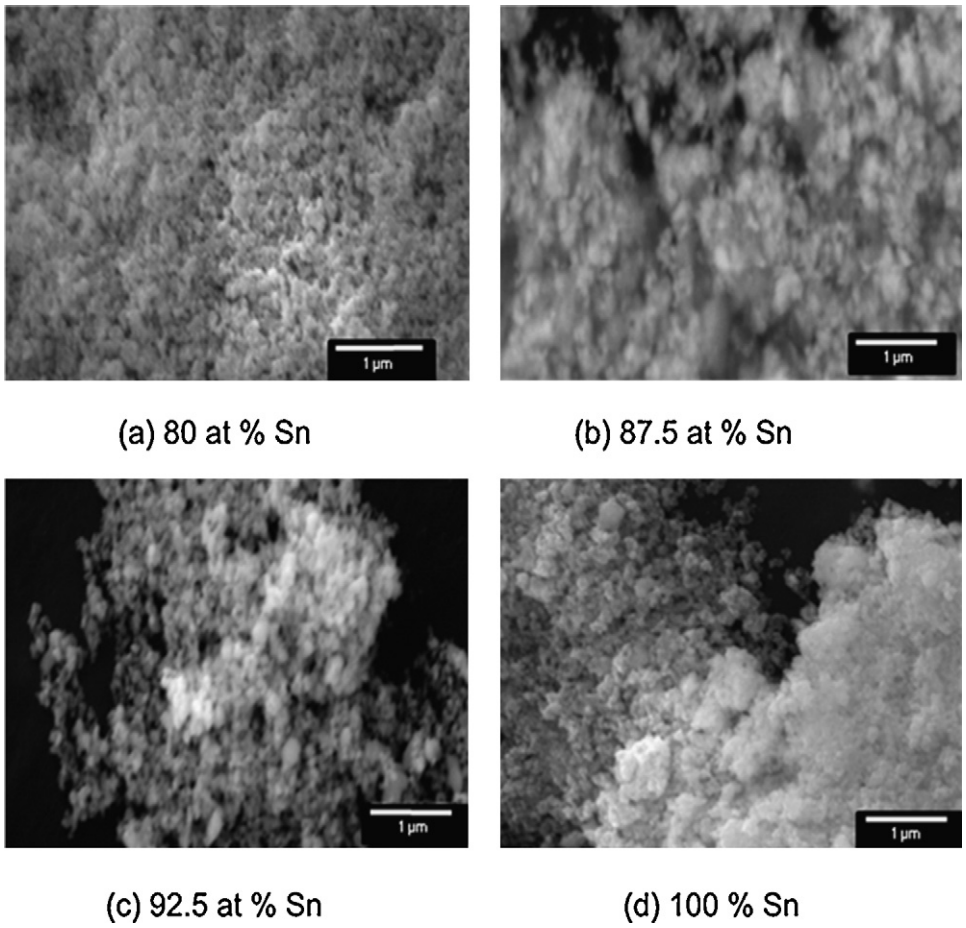

Fig. 2. SEM pictures as examples of four nano-sized samples containing 80, 87.5, 92.5, and 100 at% Sn, as prepared and without any further treatment.

and 2 °C according to average particle sizes of 50, 55, 70, 95, 105, 120, and 135 nm, respectively. Fig. 6 shows the variation of ΔT with particle size. This is in quite good agreement with previous reports on the reduction of the melting temperature with decreasing particle size for pure Sn [26] or different lead-free solder alloys, e.g. Sn–3.0Ag–0.5Cu [27] or Sn–0.4Co–0.7Cu [28].

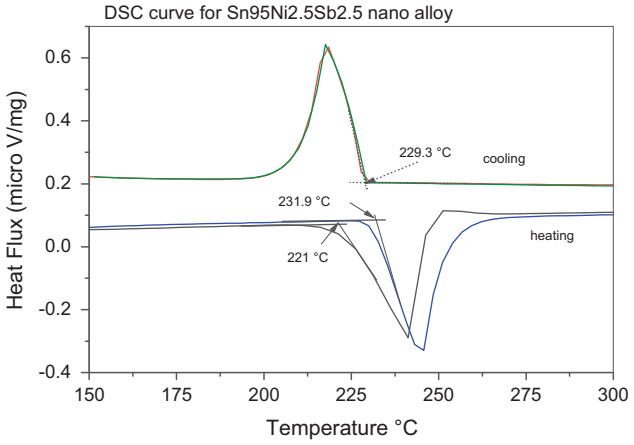

Fig. 3. DSC curves on first and second heating for a nano-crystalline sample with the composition $Sn_{95}Ni_{2.5}Sb_{2.5}$.

It is also interesting to compare the observed melting temperature depression with the equation given by Qi and Wang [15]:

$$T_m = T_{mb}\left(1 - 6\alpha\frac{r}{D}\right) \quad (1)$$

where T_m and T_{mb} are the melting temperatures of the nanoparticles and of the bulk material, α is a shape factor, r is the atomic radius, and D is the diameter of the nanocrystals. Assuming spherical particles ($\alpha = 1$), and taking the melting point (505 K) and the atomic radius of pure metallic Sn ($r = 0.140$ nm [29]) – although it is clear that the samples contain some small amounts of Ni_3Sn_4 and that Sn has dissolved some Sb – a curve can be calculated which is included in Fig. 6. Considering the fact that the particle sizes estimated from SEM micrographs may contain errors in the range of ±10–15% and that the melting temperatures are not for pure Sn, the agreement with the experimental results is still quite good.

3.2. Determination of the excess surface energy of nanoalloys

To determine the excess surface energy of nano-crystalline samples with different particle sizes, individual parts of the sample $Sn_{95}Ni_{2.5}Sb_{2.5}$ that had been annealed at 180 °C for different periods of time (see above) were dropped from room temperature (299 ± 0.5 K) into the calorimeter which was kept at 573 K. A piece of the sample that had been heated twice up to 773 K during thermal cycling in the DSC was used as the reference bulk sample after surface cleaning.

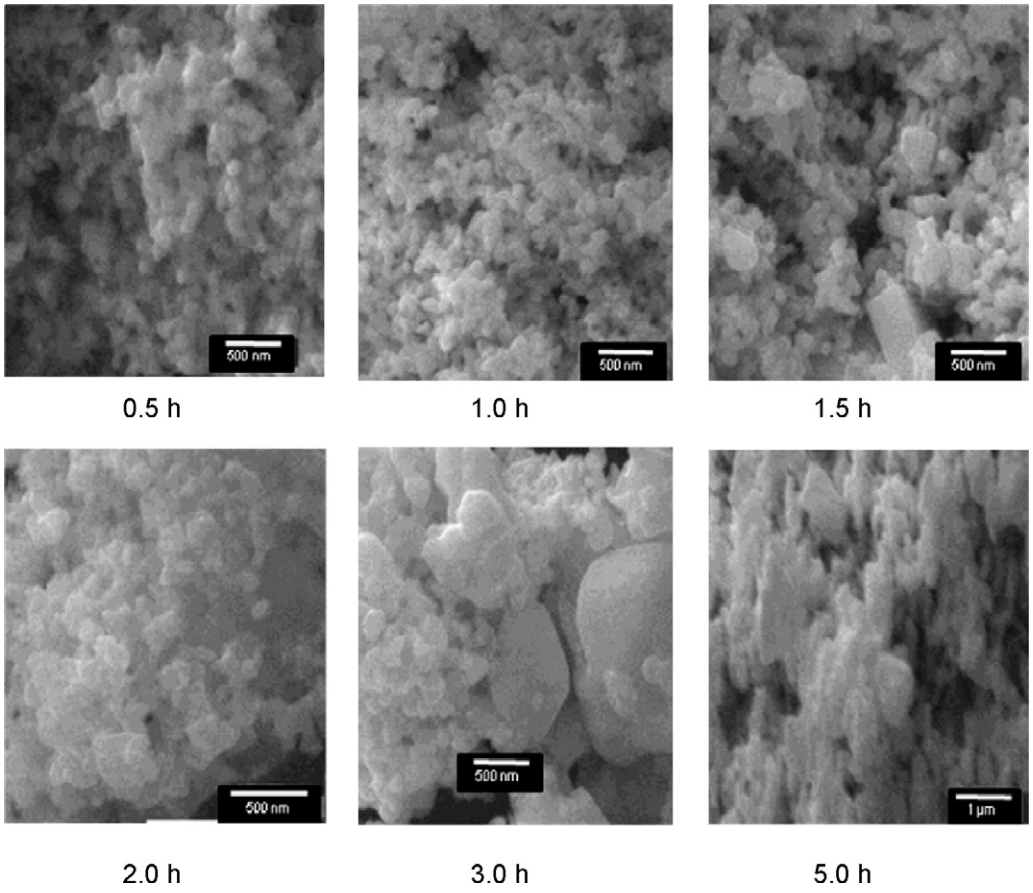

Fig. 4. SEM pictures of a nano-crystalline sample with the composition $Sn_{95}Ni_{2.5}Sb_{2.5}$ heated at 180 °C for 0.5, 1.0, 1.5, 2.0, 3.0, and 5.0 h.

Dropping of a sample into the calorimeter resulted in an endothermic peak which was observed in the heat flux versus time plot. This endothermic effect is due to the difference in enthalpy content (H_{573}–H_{299}) which is itself composed of the enthalpy difference of the solid sample between 299 K and the melting temperature T_m ($\int_{299}^{Tm} \Delta C_p^{solid} \cdot dT$), the enthalpy effect due to the melting process itself, the enthalpy difference of the liquid sample between the end of the melting process and the calorimeter temperature 573 K, and an additional exothermic heat effect ($^{ex}\Delta H$) due to the conversion of nano-size samples to the bulk samples.

A steady base line in the heat flux versus time curve after 30 min indicated that the above thermal effects were completed within this time period. The values of the enthalpy change for dropping of the different nano-alloys were obtained by integrating the area under the curve over a time scale between 100 and 1800 s after the sample drop. Table 2 gives the (H_{573}–H_{299}) values in J g^{-1} for the $Sn_{95}Ni_{2.5}Sb_{2.5}$ alloy with average particle sizes ranging from 50 to 135 nm. From this table it can be observed that the (H_{573}–H_{299}) values decrease with a decrease in the particle size of the alloys. This is attributed to the exothermic effect arising from the conversion of nano-particles to bulk material which has to become larger if the particles become smaller. The excess surface enthalpy stored in the nano-particles is released when the alloy is heated

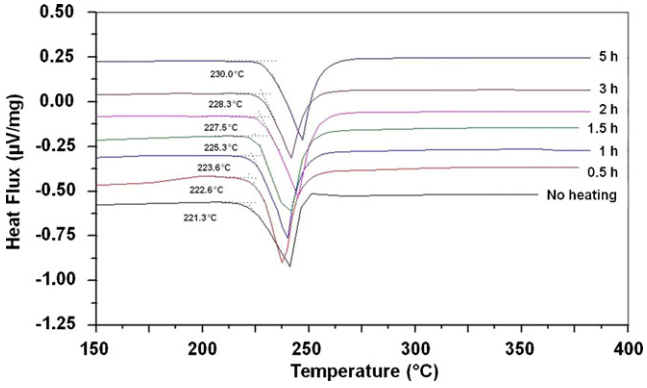

Fig. 5. DSC curves for a nano-crystalline sample with the composition $Sn_{95}Ni_{2.5}Sb_{2.5}$ heated at 180 °C in quartz ampoules for periods of 0.5, 1.0, 1.5, 2.0, 3.0, and 5.0 h.

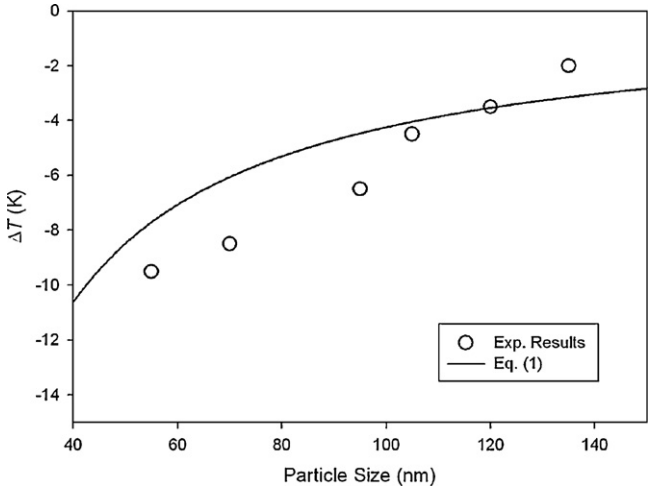

Fig. 6. Depression of the onset temperature of the first melting peak versus particle size for a nano-crystalline sample with the composition $Sn_{95}Ni_{2.5}Sb_{2.5}$.

Table 2
Depression in the onset temperature of the melting peak (ΔT) of nano-crystalline $Sn_{95}Ni_{2.5}Sb_{2.5}$ samples as a function of particle size (obtained from SEM micrographs) and their excess surface energy.

Annealing time (h)	Average particle size (nm)	ΔT (K)	$(H_{573}-H_{299})$ (J g^{-1})	Excess enthalpy (J g^{-1})
	Bulk	–	129,342 ± 1275	–
0	50	11	110,496 ± 1438	−18,846 ± 1921
0.5	55	9.5	111,310 ± 1249	−18,032 ± 1784
1	70	8.5	117,510 ± 658	−11,832 ± 1434
1.5	95	6.5	124,576 ± 1602	−4766 ± 2047
2	105	4.5	127,838 ± 723	−1504 ± 1465
3	120	3.5	128,297 ± 85	−1045 ± 1277
5	135	2	128,523 ± 613	−819 ± 1414

and undergoes melting. The average excess energy of the different nano-crystalline samples was obtained by subtracting their $(H_{573}-H_{299})$ values from that of the bulk sample. It was found to be 18.8 ± 1.9, 18.0 ± 1.8, 11.8 ± 1.4, 4.8 ± 2.0, 1.5 ± 1.5, 1.0 ± 1.2 and 0.8 ± 1.4 kJ g^{-1} for $Sn_{95}Ni_{2.5}Sb_{2.5}$ samples with average particle sizes of 50, 55, 70, 95, 105, 120 and 135 nm, respectively (see Table 2).

4. Conclusions

Ni–Sb–Sn nanoalloys with compositions between 80.0 and 97.5 at% Sn were synthesized by reduction of metal chloride solutions with $NaBH_4$ in alkaline medium. In the obtained products, the presence of Sn and of small amounts of the binary phases Ni_3Sn_4 and SbSn (β-phase) could be established at 0 °C. The particle size of the alloys progressively decreases with a decrease in Sn content. A relative decrease in melting temperature of up to 15 °C compared to the bulk sample was observed for the different alloys depending on their particle size. Finally, the excess surface energy of the nanoalloys was determined as a function of particle size and was found to increase with decreasing particle size.

Acknowledgements

This paper is a contribution to the European COST Actions MP 0602 and MP 0903. Financial support by the European Union through a Marie Curie Fellowship for R.M. (FP7-PEOPLE-IIF-2008, Project No.234920), by the Ministry of Education, Youth and Sports of the Czech Republic (Grants No. LD 11024 and MEB 061005), as well as additional support by the Scientific-Technical Cooperation Austria-Czech Republic (Project CZ 08/2010) is gratefully acknowledged.

References

[1] H. Gleiter, Prog. Mater. Sci. 33 (1989) 223–315.
[2] R. Dingreville, J. Qu, M. Cherkaoui, J. Mech. Phys. Solids 53 (2005) 1827–1854.
[3] R.S. Ningthoujam, N. Sudhakar, K.P. Rajeev, N.S. Gajbhiye, J. Appl. Phys. 91 (2002) 6051–6056.
[4] J.R. Sambles, Proc. R. Soc. Lond. Ser. A 324 (1971) 339–351.
[5] A.N. Goldstein, C.M. Echer, A.P. Alivisatos, Science 256 (1992) 1425–1427.
[6] H.W. Sheng, K. Lu, E. Ma, Nanostruct. Mater. 10 (1998) 865–873.
[7] K.F. Peters, J.B. Cohen, Y.-W. Chung, Phys. Rev. B 57 (1998) 13430–13438.
[8] C.L. Cleveland, W.D. Luedtke, U. Landman, Phys. Rev. B 60 (1999) 5065–5077.
[9] P. Pawlow, Z. Phys. Chem. 65 (1909) 545–548.
[10] Ph. Buffat, J.-P. Borel, Phys. Rev. A 13 (1976) 2287–2298.
[11] J.-P. Borel, Surf. Sci. 106 (1981) 1–9.
[12] K. Dick, T. Dhanasekaran, Z. Zhang, D. Meisel, J. Am. Chem. Soc. 124 (2002) 2312–2317.
[13] K.K. Nanda, S.N. Sahu, S.N. Behera, Phys. Rev. A 66 (2002) 13208/1–13208/8.
[14] Q. Jiang, S. Zhang, M. Zhao, Mater. Chem. Phys. 82 (2003) 225–227.
[15] W.H. Qi, M.P. Wang, Mater. Chem. Phys. 88 (2004) 280–284.
[16] Y.-W. Du, M.-X. Xu, J. Wu, Y.-B. Shi, H.-X. Lu, J. Appl. Phys. 70 (1991) 5903–5905.
[17] D. Zhang, K.J. Klabunde, C.M. Sorensen, G.C. Hadjipanayis, Phys. Rev. B 58 (1998) 14167–14170.
[18] F. Shir, L. Yanik, L.H. Bennett, E. Della Torre, R.D. Shull, J. Appl. Phys. 93 (2003) 8295–8297.
[19] J. Del Castillo, V.D. Rodríguez, A.C. Yanes, J. Mendez-Ramos, M.E. Torres, Nanotechnology 16 (2005) S300–S303.
[20] A.C. Yanes, J. Del Castillo, M. Torres, J. Peraza, V.D. Rodríguez, J. Mendez-Ramos, Appl. Phys. Lett. 85 (2004) 2343–2345.
[21] http://heraeus-contactmaterials.com/en/products/solderpowder/productp_solderpowder.aspx.
[22] R. Yang, J. Huang, W. Zhao, W. Lai, X. Zhang, J. Zheng, X. Li, J. Power Sources 195 (2010) 6811–6816.
[23] TOPAS V3, General Profile and Structure Analysis Software for Powder Diffraction Data, Bruker AXS, Karlsruhe, Germany, 2005.
[24] H. Flandorfer, F. Gehringer, E. Hayer, Thermochim. Acta 382 (2002) 77–87.
[25] R. Mishra, A. Zemanova, A. Kroupa, H. Ipser, in preparation.
[26] Ch.-D. Zou, Y.-L. Gao, B. Yang, Q.-J. Zhai, Trans. Nonferrous Met. Soc. China 20 (2010) 248–253.
[27] Ch.D. Zou, Y.L. Gao, B. Yang, Q.J. Zhai, X.Zh. Xia, Q.J. Zhai, C. Andersson, J. Liu, J. Electron. Mater. 38 (2009) 351–355.
[28] Ch.D. Zou, Y.L. Gao, B. Yang, Q.J. Zhai, Q.J. Zhai, C. Andersson, J. Liu, Sold. Surf. Mount Technol. 21 (2009) 9–13.
[29] C.E. Housecroft, A.G. Sharpe, Inorganic Chemistry, 3rd ed., Pearson Education Ltd., Harlow, UK, 2008, p. 381.